IEEE Access
Multidisciplinary | Rapid Review | Open Access Journal

Received June 11, 2021, accepted June 18, 2021, date of publication June 24, 2021, date of current version July 1, 2021.

Digital Object Identifier 10.1109/ACCESS.2021.3092145

A Modified Manta Ray Foraging Optimizer for Planning Inverter-Based Photovoltaic With Battery Energy Storage System and Wind Turbine in Distribution Networks

H. ABDEL-MAWGOUD[1], ABDELFATAH ALI[2], SALAH KAMEL[1], CLAUDIA RAHMANN[3], AND ABDEL-MOAMEN M. A.[4]

[1]Department of Electrical Engineering, Faculty of Engineering, Aswan University, Aswan 81542, Egypt
[2]Department of Electrical Engineering, Faculty of Engineering, South Valley University, Qena 83523, Egypt
[3]Department of Electrical Engineering, University of Chile, Santiago 80000, Chile
[4]Department of Electrical Engineering, Faculty of Energy Engineering, Aswan University, Aswan 81528, Egypt

Corresponding authors: Abdel-Moamen M. A. (abdelmoamen@energy.aswu.edu.eg) and Salah Kamel (skamel@aswu.edu.eg)

This work did not involve human subjects or animals in its research.

ABSTRACT It is widely accepted that the integration of natural sources in distribution networks is becoming more attractive as they are sustainable and nonpolluting. This paper firstly proposes a modified Manta Ray Foraging Optimizer (MMRFO) to enhance the characteristic of MRFO technique. The modified MRFO technique is based on inserting the Simulated Annealing technique into the original MRFO to enhance the exploitation phase which is responsible for finding the promising region in the search area. Secondly, the developed technique is utilized for determining the best sizes and locations of multiple wind turbine (WT) and photovoltaic (PV) units in Radial Distribution System (RDS). The total system loss is taken as single-objective function to be minimized, considering the probabilistic nature of PV and WT output generation with variable load demand. Reactive loss sensitivity factor (QLSF) is utilized for obtaining the candidate locations up to fifty percent of total system buses with the aim of reducing the search space. Battery Energy Storage System (BESS) is used with PV to change it into a dispatchable supply. The changes in system performance by optimally integrating PV and WT alone or together are comprehensively studied. The proposed solution approach is applied for solving the standard IEEE 69 bus RDS. The obtained results demonstrate that installing PV and WT simultaneously achieves superior results than installing PV alone and WT alone in RDS. Further, simultaneous integration of WT and PV with BESS gives better results than simultaneous integration of WT and PV without BESS in RDS. The simulation results prove that the total system losses can be reduced by enabling the reactive power capability of PV inverters. The convergence characteristic shows that the modified MRFO gives the best solutions compared with the original MRFO algorithm.

INDEX TERMS Battery energy storage, distribution network, Manta ray foraging optimization, optimization, photovoltaic, uncertainty, wind turbine.

NOMENCLATURE

ACRONYMS

PV	photovoltaic
WT	wind turbine
BESS	battery energy storage system
RDS	radial distribution system
MRFO	manta ray foraging optimizer
MMRFO	modified manta ray foraging optimizer
SA	Simulated annealing
QLSF	reactive loss sensitivity factor
PDFs	probability distribution functions
WOA	whale optimization algorithm
KHA	krill herd algorithm
BSOA	backtracking search optimization algorithm
PSO	Particle swarm optimization

The associate editor coordinating the review of this manuscript and approving it for publication was Lasantha Meegahapola.

FFA	firefly algorithm
GA	genetic algorithm
CSA	cuckoo search algorithm
GWO	grey wolf optimizer
ABC	artificial bee colony
MOCD	Multi-objective opposition based chaotic differential evaluation

INDICES AND SETS

r	index of buses in RDS
e	index of branches in RDS
L	index of PVs
m	index of WTs
n	index of BESSs
N_{B}	set of buses in RDS
N_{Br}	set of branches in RDS
N_{PV}	set of PVs in RDS
N_{WT}	set of WTs in RDS
N_{BESS}	set of BESSs in RDS

PARAMETERS

n_a	active load modeling voltage index
n_r	reactive load modeling voltage index
Z, q	Shape and scale parameters of Weibull function
σ_s, μ_s	Standard deviation and mean of the wind velocity
x_{co}, x_{ci}	cut-off and cut-in velocities of WT
x_r	rated velocity of WT
P_{rated}, x_m	rated power and average velocity of WT
P, φ	parameters of beta distribution function
ϑ, γ	standard deviation and mean of solar irradiance
N	total number of PV modules
K_u	current temperature coefficient in ampere per Celsius
K_o	voltage temperature coefficient in voltage per Celsius
T_m, T_e	the ambient and cell temperature in Celsius
N_n	the nominal temperature of cell in Celsius
V_o, I_s	open-circuit voltage and short circuit current
P_b	the high output generation of PV unit
η_d, η_a	discharging and charging efficiencies of BESS
η_{BESS}	the round-trip efficiency of BESS
ΔT	represents the time duration
Q	boltzmann probability
b, b_1	represent a random number among [0,1]
$\propto$, β	represent a weight coefficient
S	solar irradiance
V_{Up}, V_{Do}	The maximum and minimum allowable operating bus voltage
$P_{WT,H}$, $P_{WT,L}$	the upper and lower values of WT output power
$P_{PV,H}$, $P_{PV,L}$	the upper and lower magnitudes of PV output
$E_{BESS,L}$, $E_{BESS,H}$	the lower and upper magnitudes of BESS energy
$I_{max,e}$	the high limiting current of branch (e)
$X_{1,2}$, $R_{1,2}$	the reactance and resistance among buses # 1 and # 2
$Q_{L,2}$, $P_{L,2}$	the reactive and active loads at bus # 2

FUNCTIONS AND VARIABLES

F_k (s)	the Beta distribution function of the solar irradiance (s)
F_j (x)	the Weibull probability density function of the wind speed (x)
F_{obj}	the main objective function
P_{loss} (t)	represents the power losses at time t
Q_1, P_1	The reactive power and real power among buses # 1 and # 2
V_1, V_2	the voltage value of bus # 1 and bus # 2
P_{PV}, P_{WT}, and P_{BESS}	the generated active power of PV, WT, and BESS
P_0, Q_0	the injected active and reactive power from substation
I_b	The current in the branch (b)
$S_{inverter}$	the rated power of the PV inverter
$P^d_{BESS,m}$	the discharging power of BESS
$P^a_{BESS,m}$	The charging power of BESS
$E^d_{BESS,m}$	the discharging energy of BESS
$E^a_{BESS,m}$	The charging energy of BESS
P^d_i, P^d_{best}	the positions of manta ray and plankton

I. INTRODUCTION

Energy can be known as a key factor for the social and economic growth. Most global energy is supplied from fossil fuels such as oil, coal and natural gas that are used in most worldwide power stations. The power generation of worldwide power stations that is based on fossil fuels is around seventy-five percent of global power generation [1]–[3]. However, countries around the world have started to decrease their reliance on fossil fuel because of energy security and environmental issues [4]–[7]. In this way, during the last years there has been a trend to cover the increase in electrical load demand by integrating renewable energy sources (RES) in distribution networks as these sources are clean and more sustainable compared to fossil fuels [8]–[11]. There are different types of RES that are used in power systems such as wind turbine (WT), hydropower, photovoltaic (PV), and biomass [12]–[14].

The PV technology converts solar energy into electrical energy. In the last decade, this technology has rapidly

developed and its price has dropped exponentially, so its integration in Radial Distribution Systems (RDS) is becoming popular [15], [16]. However, PV generation is a non-dispatchable source as its output power depends on weather conditions [17], [18]. Still, the PV generation can be installed with a BESS to reduce its uncertainty and turn it into a dispatchable source [19]–[24]. In this sense, the BESS injects active power to the system as long as the PV power generation is zero or small on the night [25], [26] and charges during the day as long as the PV output power is more than the required load. Interfacing inverter of PV generation is utilized to inject/absorb reactive power to/from grid for voltage regulation and power losses minimization.

WT converts the wind energy into electrical energy and its output depends on the wind velocity. Installing WT in RDS is encouraged to rise the system reliability and stability as it is able to carry the load at transient conditions due to its inertia [27]. A WT starts and stops running as long as the wind velocity exceeds the cut-in value and cut-out magnitude, respectively. Also, a WT generates power as long as the wind velocity overrides its rated value.

From the literature, the power generation of renewable sources such as PV and WT are dependent on natural conditions, hence their uncertainties should be taken into account while determining their optimal allocations power system. The uncertainties of PV and WT have been considered using Beta and Weibull probability distribution functions (PDFs) [28], [29].

Recently, several researchers studied the integration of inverter-based PV, WT, and BESS in distribution systems through many aspects such as planning, design, energy management, and optimization [30]–[32]. Also, many techniques studied the optimal placement and sizing of WT and PV with BESS. In [33], [34], Genetic algorithm (GA) has been applied for determining the optimal sizing of BES and PV in distribution network with the aim of minimizing the cost of energy generated, voltage deviation and system loss. In [35], Linear programming (LP) has been used for energy storage dispatch of PV with BES connected in a grid. Whale Optimization Algorithm (WOA) has been applied for obtaining the sizing of electric vehicle station combined with PV and battery for minimizing the system cost [36], and for obtaining the size of batteries in RDS for minimizing the system loss in [37]. Modified henry gas solubility optimization algorithm (modified HGSO) has been applied for determining the optimal sizing of battery with PV in RDS for minimizing the system loss during 24-hours in [38]. Grey Wolf Optimizer algorithm (GWO) has been used for determining the sizing of battery with PV and WT for minimizing annual energy loss in [39], and for obtaining the size of batteries in RDS for minimizing the annual cost of the system in [40]. Harris hawks optimizer-particle swarm optimization (HHO-PSO) has been suggested for optimal sizing of PV and WT for maximizing the techno economic benefits in [41]. Particle Swarm Optimization (PSO) algorithm has been developed for determining the optimal allocation of battery in RDS to decrease annual operation cost of the system [42]. The optimal sizing of inverter with WT and electric vehicle using GWO algorithm for minimizing system energy loss has been presented in [43]. Although metaheuristic techniques are efficient in solving different optimization problems, they may require more simulation time in complex optimization problems. Therefore, efforts have been made to solve this drawback and improve the performance of metaheuristic techniques in obtaining global solutions in less simulation time than the original algorithms.

Simulated Annealing (SA) is an efficient algorithm which is created by the cc [44]. This agorithm is simulated by updating the temperature at each iteration to simulate the annealing process. Also, SA is based on the Boltzmann probability, which is applied to give an efficient exploration in the search area by controlling the updating location of agents. MRFO is a new metaheuristic optimization algorithm that simulates the foraging behavior of manta ray [45]. Manta ray is cold-blooded fish with a pair of pectoral fins and a flat diamond-shaped body. The types of manta rays that are living in oceans are reef manta rays and giant manta rays. There are three mathematical models created in the MRFO algorithm to simulate the foraging behaviors of a manta ray, somersault foraging, cyclone foraging and chain foraging.

This paper presents an efficient modified algorithm by inserting the SA technique into the MRFO technique to enhance the exploitation phase of the MRFO technique. The MRFO technique is modified to improve its characteristics and to be able to get the global solutions at less search agent. The obtained result proved that the modified technique is better than the original one in determining the best global solution with less simulation time. The modified technique can be utilized to obtain the best sizes and locations of inverter-based PV, WT and PV without/with BESS. The effects of enabling reactive power capability of PV inverters in the reduction of system power losses is also studied. The optimal allocation of inverter-based PV, WT, and BESS is obtained using the stochastic nature of WT and PV generation with variable load demand. Integration of WT and PV with BESS considering reactive power capability of PV inverters enhances the system power equality, enhance the grid voltages, increases the system capacity, and reduces system loss. Also, the contributions of this paper are defined as follows:

- Proposing a modified version of MRFO technique (M MRFO).
- Determining the optimal allocation of WT and PV without/with BESS in RDS using the stochastic nature of WT and PV generation with variable load demand.
- Studying the effect of enabling the reactive power capability of PV inverters on system power losses.
- The total energy loss is defined as single-objective function.
- Investigating the changes in system voltage profile and system loss by integrating WT and PV without/with BESS in RDS.

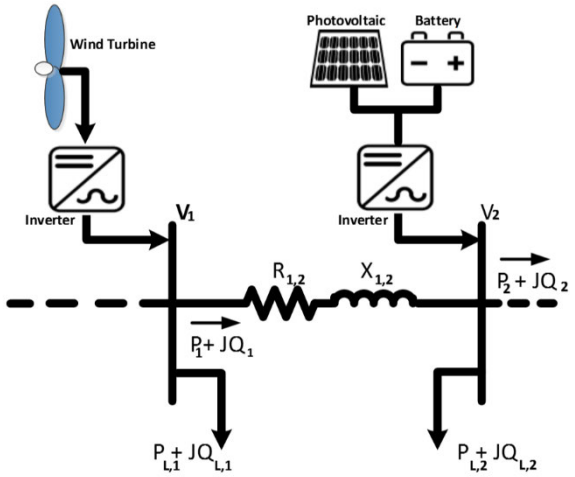

FIGURE 1. Representation of two buses in distribution system.

This paper can be structured as follows: Section II presents the objective function and problem constraints. The load modeling, PV modeling, WT modeling, BESS modeling, and inverter-based PV are introduced in Section III. Section IV explains the modified MRFO algorithm. The obtained results are discussed clearly in Section V. Section VI report the conclusion of paper.

II. PROBLEM FORMULATION

The represented section of the main feeder in the distribution network is illustrated in Fig. 1.

The load flows of a distribution system can be obtained by a forward-backward sweep algorithm [46]. The reactive and real load flows through the branches is evaluated in a backward direction as follows:

$$P_1 = P_2+P_{L,2}+R_{1,2}\left(\frac{(P_2+P_{L,2})^2+(Q_2+Q_{L,2})^2}{|V_2|^2}\right) \quad (1)$$

$$Q_1 = Q_2+Q_{L,2}+X_{1,2}\left(\frac{(P_2+P_{L,2})^2+(Q_2+Q_{L,2})^2}{|V_2|^2}\right) \quad (2)$$

where, $X_{1,2}$, Q_1, $R_{1,2}$ and P_1 are the reactance, reactive power, resistance and real power between among buses # 1 and # 2, respectively. $Q_{L,2}$ and $P_{L,2}$ are the reactive and active loads at bus # 2, respectively.

The voltage at bus # 2 can be calculated in the forward direction as follows:

$$V_2^2 = V_1^2 - 2(P_1R_{1,2}+Q_1X_{1,2})+(R_{1,2}^2+X_{1,2}^2)\left(\frac{P_1^2+Q_1^2}{V_1^2}\right) \quad (3)$$

where, V_1 is the voltage value of bus # 1 and V_2 is the voltage value of bus # 2, respectively.

The real power flow through the branches will be changed because of the output power from PV, WT, and BESS that are integrated in RDS. Also, the reactive load flow through the branches will be changed because of the output power from PV inverter. Therefore, the reactive and real load flows equations are updated as:

$$P_1 = P_2+P_{L,2}+R_{1,2}\left(\frac{(P_2+P_{L,2})^2+(Q_2+Q_{L,2})^2}{|V_2|^2}\right) - P_{DG} \quad (4)$$

$$Q_1 = Q_2+Q_{L,2}+X_{1,2}\left(\frac{(P_2+P_{L,2})^2+(Q_2+Q_{L,2})^2}{|V_2|^2}\right) \pm Q_{PV} \quad (5)$$

where,

$$P_{DG} = P_{PV} + P_{WT} + P_{BESS} \quad (6)$$

P_{PV}, P_{WT} and P_{BESS} are the generated active power of PV, WT, and BES, respectively, Q_{PV} represents the reactive power absorbed/ injected through PV inverter.

The main objective function is the total system loss.

$$F_{obj} = Min\left(\sum_{t=1}^{24} P_{loss}(t)\right) \quad (7)$$

where, $P_{loss}(t)$ represents the power losses at time t.

The inequality and equality constraints are introduced as follows [47]–[49]:

A. EQUALITY CONSTRAINTS

These constraints include load flow and balance equations. Eq. (8) describes the active power balance among the active power consumption and the active power supplied to the system by the substation, PV, WT, and BESS.

$$P_o + \sum_{L=1}^{N_{PV}} P_{PV}(L) + \sum_{m=1}^{N_{WT}} P_{WT}(m) + \sum_{n=1}^{N_{BESS}} P_{BESS}(n) = \sum_{r=1}^{N_B} P_L(r) + \sum_{e=1}^{N_{Br}} P_{Loss}(e) \quad (8)$$

$$Q_o + \sum_{L=1}^{N_{PV}} Q_{PV}(L) = \sum_{r=1}^{N_B} Q_L(r) + \sum_{e=1}^{N_{Br}} Q_{Loss}(e) \quad (9)$$

where, $P_L(r)$ and $Q_L(r)$ are the real and reactive loads at bus (r). N_{PV}, N_{WT}, N_{BESS} are the number of PV, WT and BESS units, respectively. N_B, and N_{Br} are the number of buses and branches, respectively. The reactive and active power losses of branch (e) are $Q_{Loss}(e)$ and $P_{Loss}(e)$, respectively. The injected reactive and active power from the substation are P_o and Q_o, respectively.

B. INEQUALITY CONSTRAINTS

1) BUS VOLTAGES CONSTRAINTS

These constraints should be kept among the minimum and maximum limits of the system voltage, as given in (10).

$$V_{Do} \le V_r \le V_{Up} \quad (10)$$

where, V_r represents the voltage of bus (r) which can be operated among the maximum magnitude V_{Up} and minimum value V_{Do}.

2) PV+ BESS AND WT SIZING LIMITS

The sizing limits of PV+BESS and WT units are given as:

$$\left(\sum_{L=1}^{N_{PV}} P_{PV}(L) + \sum_{m=1}^{N_{WT}} P_{WT}(m) + \sum_{n=1}^{N_{BESS}} P_{BESS}(n)\right) \leq \left(\sum_{r=1}^{N_B} P_L(r) + \sum_{e=1}^{N_{Br}} P_{Loss}(e)\right) \quad (11)$$

$$\sum_{L=1}^{N_{PV}} Q_{PV}(L) \leq \left(\sum_{r=1}^{N_B} Q_L(r) + \sum_{e=1}^{N_{Br}} Q_{Loss}(e)\right) \quad (12)$$

$$P_{PV,L} \leq P_{PV,r} \leq P_{PV,H} \quad (13)$$

$$P_{WT,L} \leq P_{WT,r} \leq P_{WT,H} \quad (14)$$

$$E_{BESS,L} \leq E_{BESS,r} \leq E_{BESS,H} \quad (15)$$

where, $P_{WT,H}$ and $P_{WT,L}$ are the upper and lower values of WT output power, respectively. $P_{PV,H}$ and $P_{PV,L}$ represent the upper and lower magnitudes of PV output, respectively. $E_{BESS,L}$ and $E_{BESS,H}$ are the lower and upper magnitudes of BESS energy.

3) LINE CAPACITY LIMITS

The branches current is operating under operating constraints [50].

$$I_b \leq I_{\max,e} \quad b = 1, 2, \ldots, N_{Br} \quad (16)$$

where, $I_{\max,e}$ is the high limiting current of branch (b).

III. MODELING OF PV+BESS AND WT

A. LOAD MODELING

System load is modeled as a commercial load during 24-hours daily, as shown in Fig. 2 [51]. This model is based on a time-varying during 24-hours and voltage-dependent load [52]. Therefore, the commercial load can be modeled according to the following equations.

$$P_u(h) = P_{L,u}(h) \times V_u^{n_a} \quad (17)$$

$$Q_u(h) = Q_{L,u}(h) \times V_u^{n_r} \quad (18)$$

where, Q_u and P_u represent the reactive and real power injections at bus (u), $Q_{L,u}$and $P_{L,u}$ are the reactive and real loads at bus (u), n_r and n_a are the reactive and active load modeling voltage indexes (1.51 and 3.4, respectively [52]).

IV. WT MODELING

The output power of WT is based on wind velocity. The Weibull probability density function is used to model the probabilistic of the wind velocity. The Weibull probability density function $F_j(x)$ of the wind speed (x) is calculated as:

$$F_j(x) = \frac{z}{q}\left(\frac{x}{q}\right)^{z-1} \exp\left[-\left(\frac{x}{q}\right)^z\right] \quad (19)$$

where, z and q represent the shape and scale parameters, respectively. Several approaches are utilized for calculating the parameters q and z [28], [53], [43]. Here, they are determined based on the standard deviation σ_s and mean (μ_s) of the wind velocity as given in (20) and (21).

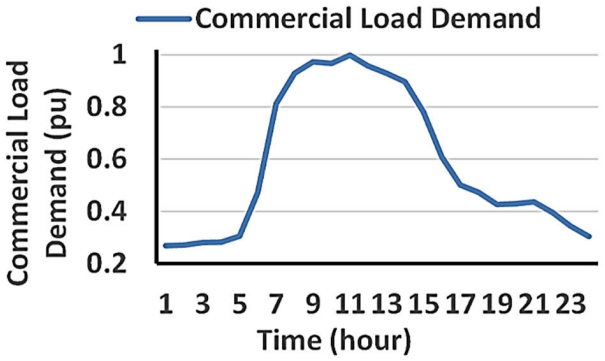

FIGURE 2. Commercial load during 24-hours daily.

$$z = \left(\frac{\sigma_s}{\mu_s}\right)^{-1.086} \quad (20)$$

$$q = \frac{\mu_s}{\Gamma(1 + (1/k))} \quad (21)$$

The output power of WT is calculated through the WT characteristics as follows:

$$P_j(x_m) = \begin{cases} 0, & 0 \leq x_m < x_{ci} \\ P_{rated} \times \dfrac{(x_m - x_{ci})}{(x_r - x_{ci})}, & x_{ci} \leq x_m < x_r \\ P_{rated}, & x_r \leq x_m < x_{co} \\ 0, & x_m \geq x_{co} \end{cases} \quad (22)$$

where, x_r, x_{co} and x_{ci} describe, respectively, the rated velocity, cut-off velocity and cut-in velocity of WT; P_{rated} and x_m represent, respectively, the rated power and average wind velocity of WT; $P_W(x_m)$ represents the power generation of WT. The average output power of WT ($P_{W,\,av}$) for a period (t) can be then calculated as:

$$P_{W,\,av} = \int_0^t P_W(x_m) F_W(x) dx \quad (23)$$

A. PV MODELING

PV output is based on solar irradiance. The PV modeling can be implemented as in [29]. The model of PV can be evaluated using Beta function as shown in (24). Also, Beta function is based on standard deviation and mean of solar irradiance that can be evaluated by (25).

$$F_k(s) = \begin{cases} \dfrac{\Gamma(\rho+\varphi)}{\Gamma(\rho)\Gamma(\varphi)} S^{(\rho-1)}(1-S)^{(\varphi-1)} & 0 \leq S \leq 1,\ \rho, \varphi \geq 0 \\ 0 & otherwise \end{cases} \quad (24)$$

$$\varphi = (1-\gamma)\left(\frac{\gamma(1+\gamma)}{\theta^2} - 1\right), \rho = \frac{\gamma \times \varphi}{1-\gamma} \quad (25)$$

where, $F_k(s)$ is the Beta distribution function of the solar irradiance (S). ρ and φ are the parameters of $F_k(s)$; θ and γ are the standard deviation and mean of (S).

The PV power generation is dependent on the ambient temperature and solar irradiance. The parameters of the PV module are obtained from [34]. The maximum PV output power is calculated as follows:

$$P_b(s) = N \times R \times K \times D \tag{26}$$

$$R = \frac{V_{MP} \times I_{MP}}{V_o \times I_s} \tag{27}$$

$$K = V_o - K_o \times T_c \tag{28}$$

$$D = S[I_s + K_u \times (T_c - 25)] \tag{29}$$

$$T_e = T_m + S(\frac{N_n - 20}{0.8}) \tag{30}$$

where, N is the total number of PV modules; K_u and K_o are the current and voltage temperature coefficient in ampere per Celsius and voltage per Celsius, respectively. T_m and T_e are the ambient and cell temperature in Celsius, respectively. V_o and I_s are the open-circuit voltage and short circuit current, N_n is the nominal temperature of cell in Celsius, respectively; P_b is the high output generation of the PV unit of irradiance (S). The average output of PV ($P_{PV,\ av}$) for a period (t) is then calculated as follows:

$$P_{PV,\ av} = \int_0^t P_b(s) f_k(s) ds \tag{31}$$

B. PV INVERTER

In this study, the PV inverter is enabled to absorb/inject reactive power from/to RDS. The rating of PV inverter is equal to the maximum output power of PV. During mid-day time, the real output of PV is equal to the PV rated ($S_{inverter} = P_{PV}$). Hence, the PV inverter operates at rated capacity and cannot absorb/generate reactive power from/to RDS (i.e., PV inverter works at unity power factor). When the output power of PV is not equal to its rated capacity, the remaining capacity of the PV inverter is utilized for reactive power support. The minimum and maximum reactive power which are absorbed/ injected by the PV inverter depends on the generated PV power and it is calculated by [54]:

$$Q^{\max}_{inverter} = \pm\sqrt{S^2_{inverter} - P^2_{PV}} \tag{32}$$

where $\pm Q^{\max}_{inverter}$ represents the minimum and the maximum reactive power which are injected/absorbed by the PV inverter. P_{PV} and $S_{inverter}$ are the output power generation of the PV and the rated power of the PV inverter, respectively.

C. BATTERY ENERGY STORAGE MODELING

In this work, the BESS is used with PV unit to become it into a dispatchable source. Therefore, BESS charges during the day and supply energy into grid on the night. The energy stored in the BESS (connected at bus m) at period (T) is calculated as follows [55]:

$$E_{BESS,m}(T) = E_{BESS,m}(T-1) - \frac{P^d_{BESS,m}}{\eta_d}\Delta T, \quad \text{for } P_{BESS,m}(T) > 0 \tag{33}$$

$$E_{BESS,m}(T) = E_{BESS,m}(T-1) - \eta_a P^a_{BESS,m}(T)\Delta T, \quad \text{for } P_{BESS,m}(T) \le 0 \tag{34}$$

$$\eta_{BESS} = \eta_a \times \eta_d \tag{35}$$

where, the discharging and charging efficiencies of BESS are η_d and η_a, respectively. The discharging and charging power of BESS are $P^d_{BESS,m}$ and $P^a_{BESS,m}$, respectively. η_{BESS} is the round-trip efficiency of BESS;ΔT represents the time duration.

D. SIZING OF BESS AND PV

The modified MRFO technique is applied for obtaining the optimal allocation of WT, PV, and BESS in distribution network. The BESS is located at the same best location of the PV in the distribution network. The charging and discharging energies of BESS at period (T) are calculated as follows [29]:

$$E^d_{BESS,m} = \int_0^T P^d_{BESS,m}(T)dT = \sum_{T=1}^{24} P^d_{BESS,m}(T)\Delta T \tag{36}$$

$$E^a_{BESS,m} = \int_0^T P^a_{BESS,m}(T)dT = \sum_{T=1}^{24} P^a_{BESS,m}(T)\Delta T \tag{37}$$

The combined energy of the PV and BESS connected at bus (m)($E_{(PV+BESS),m}$) and the energy of the PV (E_{PV}) can be calculated by (38) and (39) respectively:

$$E_{(PV+BESS),m} = E^g_{PV,m} + E^d_{BESS,m} \tag{38}$$

$$E_{PV,m} = E^g_{PV,m} + E^a_{BESS,m} \tag{39}$$

where, $E^g_{PV,m}$ is the injected energy from the PV into the grid. $E^d_{BESS,m}$ and $E^a_{BESS,m}$ are the discharging and charging energies of BESS, respectively. The discharging energy of the BESS can be obtained from the round-trip efficiency and its charging energy as follows:

$$E^d_{BESS,m} = \eta_{BESS} E^a_{BESS,m} \tag{40}$$

Therefore, equation (39) of the PV energy can be modified as follows:

$$E_{PV,m} = \frac{E_{(PV+BESS),m} - (1-\eta_{BESS})E^{Gr}_{PV,m}}{\eta_{BESS}} \tag{41}$$

$$P_{PV,m} = K^n_{PV} E_{PV,m} \tag{42}$$

$$K^n_{PV} = \frac{P^n_{PV}}{E^n_{PV}} \tag{43}$$

where, n represents the PV module unit.

The maximum PV output during 24-hour can be calculated by:

$$P_{PV,m} = K^n_{PV}(\frac{E_{(PV+BESS),m} - (1-\eta_{BESS})E^{Gr}_{PV,m}}{\eta_{BESS}}) \tag{44}$$

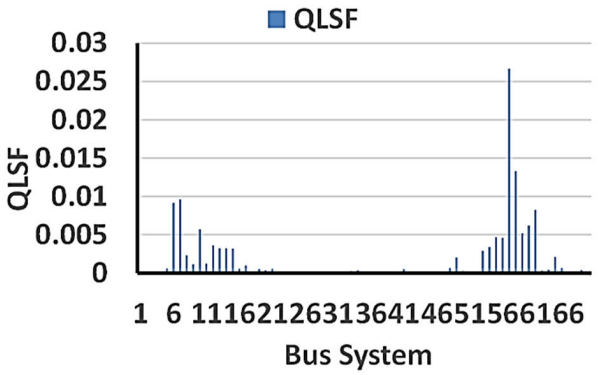

FIGURE 3. Value of QLSF for IEEE 69-bus RDS.

where, P^n_{PV} and E^n_{PV} are the maximum power and the total energy of the PV unit, respectively.

Also, the size of the BESS can be calculated as:

$$E^a_{BESS,m} = \frac{E_{(PV+BESS),m} - E^g_{PV,m}}{\eta_{BESS}} \tag{45}$$

V. REACTIVE LOSS SENSITIVITY FACTOR (QLSF)

This factor measures the sensitivity of each bus to the reactive power supplied and its effects on the real loss of RDS [21], [48], [56]. QLSF can be utilized to choose the superior candidate buses for integrating WT, PV, and BESS in RDS to reduce the simulation time and the number of search agents. In this paper, the IEEE 69-bus RDS can be utilized for planning model that consists of 68 branches and 69 buses [57]. The QLSF is calculated for each bus in the RDS using a power flow algorithm. Once the QLSF are calculated, the buses of the RDS are sorted in descending order as given by Eq. (46). The best candidate buses (considering the best 50%) are: 57, 58, 7, 6, 61, 60, 10, 59, 55, 56, 12, 54, 13, 14, 15, 53, 8, 64, 49, 11, 9, 17, 48, 65, 5, 16, 21, 19, 41, 63, 68, 34, 20 and 62 as shown in Fig.3.

$$QLSF(2) = \frac{\partial P_{Loss}(1,2)}{\partial Q_2} = R_{1,2}\left(\frac{2Q_2}{|V_2|^2}\right) \tag{46}$$

VI. MODIFIED OPTIMIZATION ALGORITHM

A. SA ALGORITHM

SA represents a metaheuristic technique that simulates the annealing process (cooling and heating process) in metal work [44]. The properties of the material can be changed by changing its internal structure due to the annealing process. SA technique is related to the temperature, which is changed at each iteration to model the annealing process. In SA algorithm, the agents can escape from the local solution and search more region of search area by the Boltzmann probability (P_{Boltz}). This probability can be utilized to control the motion direction of agents in the search space and to evaluate the ability of the agent to avoid the local solutions. The initial temperature value (R_o) is equal to 0.025 that

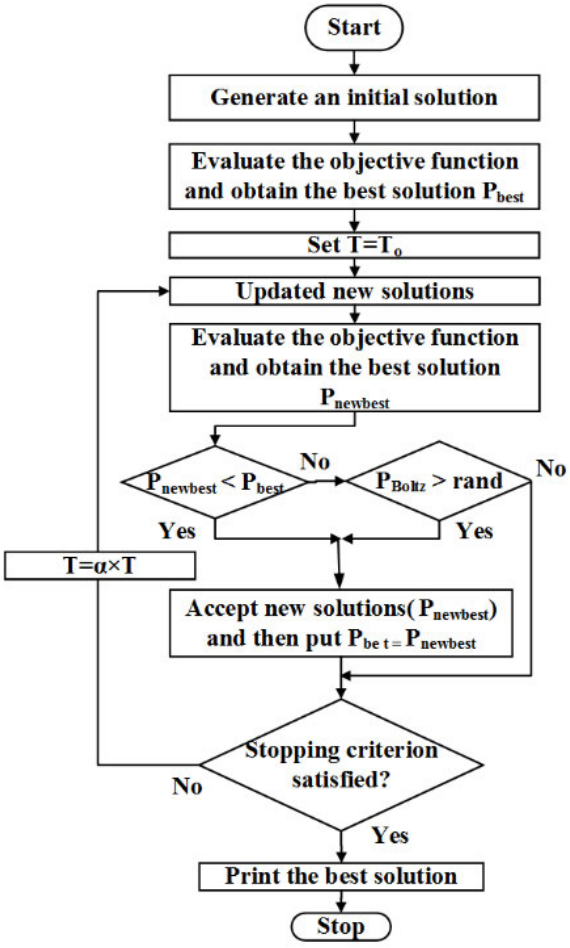

FIGURE 4. SA algorithm flowchart.

is reduced through the cooling process by Eq. (48). The Boltzmann probability can be calculated by (47). Fig. 4 illustrate the steps of SA technique in solving optimization problems.

$$Q = e^{-\frac{\varphi}{R}} \tag{47}$$

$$R = \beta \times R \tag{48}$$

where β equal to 0.99.

B. MRFO ALGORITHM

MRFO technique is simulated by the foraging behavior of manta rays when they are looking for food in the ocean. Reef manta ray and giant manta ray are the categories of manta rays which feed on plankton in the ocean. Manta ray is a cold-blooded fish with a pair of pectoral fins and a flat diamond-shaped body. Fig. 5 illustrates the steps of MRFO technique. The behaviors of MRFO technique are somersault foraging, cyclone foraging, and chain foraging, which can be modeled as follows:

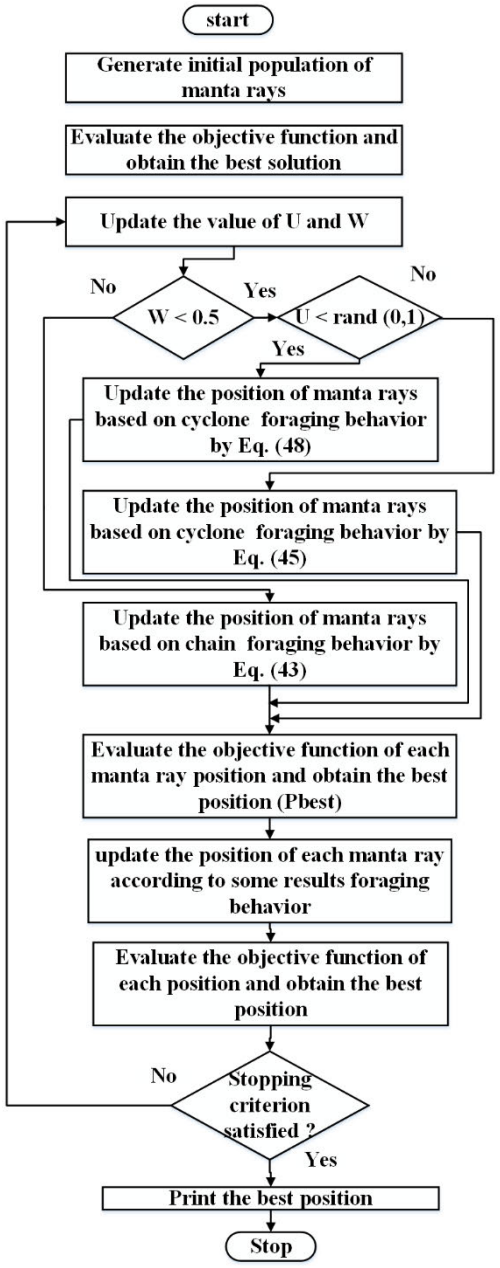

FIGURE 5. MRFO algorithm flowchart.

1) CHAIN FORAGING BEHAVIOR

At the beginning of foraging behavior, manta rays move as a chain toward the food (plankton), which can be modeled as:

$$P_i^d(z+1) = \begin{cases} P_i^d(z) + r(P_{best}^d(z) - P_i^d(z)) \\ +\alpha(P_{best}^d(z) - P_i^d(z)) \quad j = 1 \\ P_i^d(z) + r(P_{i-1}^d(z) - P_i^d(z)) \\ +\alpha(P_{best}^d(z) - P_i^d(z)) \quad j = 2, 3, \ldots, n \end{cases} \tag{49}$$

$$\alpha = 2b\sqrt{|\log(b)|} \tag{50}$$

where, b is a random number among [0, 1], α is a weight coefficient. P_i^d and P_{best}^d are the positions of manta ray and plankton, respectively.

2) CYCLONE FORAGING BEHAVIOR

The manta rays move in a spiral path around the high concentration of plankton which is represented as follows:

$$P_i^d(z+1) = \begin{cases} P_i^d(z) + r(P_{best}^d(z) - P_i^d(z)) \\ +\beta(P_{best}^d(z) - P_i^d(z)) \quad j = 1 \\ P_i^d(z) + r(P_{i-1}^d(z) - P_i^d(z)) \\ +\beta(P_{best}^d(z) - P_i^d(z)) \quad j = 2, 3, \ldots, n \end{cases} \tag{51}$$

$$\beta = 2e^{b_1 \frac{B-z+1}{B}} \sin(2\pi b_1) \tag{52}$$

The updating position of manta ray depends on the position of plankton found so far. The exploration phase of this behavior can be developed to explore more areas of search space by creating a new updating position of a manta ray which depends on the new random positions. The following equations can formulate the updating of the new position.

$$P_{rand}^d = LP^d + b(UP^d - LP^d) \tag{53}$$

$$P_i^d(z+1) = \begin{cases} P_{rand}^d(z) + r(P_{rand}^d(z) - P_i^d(z)) \\ +\beta(P_{rand}^d(z) - P_i^d(z)) \quad j = 1 \\ P_{rand}^d(z) + r(P_{i-1}^d(z) - P_i^d(z)) \\ +\beta(P_{rand}^d(z) - P_i^d(z)) \quad j = 2, 3, \ldots, n \end{cases} \tag{54}$$

where, β is the total number of iterations. b_1 is a random value among [1, 0]; β is a weight coefficient; UP^d and LP^d are the upper and lower magnitudes of the variables, respectively; P_{rand}^d represents the new random position of the manta ray.

3) SOMERSAULT FORAGING BEHAVIOR

In this behavior, manta ray performs a local, frequent, random, and cyclical movement around the plankton to optimize food intake which can be formulated as:

$$P_i^D(t+1) = P_i^D(t) + S_{som}(r_2 P_{best}^d - r_3 P_i^d(t)) \quad i = 1, 2, \ldots, N \tag{55}$$

where, S_{som} is the somersault factor equal to 2; r_2 and r_3 are random value among [1, 0].

C. MODIFIED MRFO ALGORITHM

MRFO is a Population-based technique that depends on exploitation and exploration phases. The exploration phase is used to explore the best region among all regions of the search area. The exploitation phase is used to obtain the best solution in the best region. The modified MRFO technique is proposed by inserting the SA technique into the original MRFO technique to enhance the local search in the exploitation phase, as shown in Fig. 6. In the modified MRFO technique, MRFO technique obtains the best solution and SA algorithm searches for a neighboring solution around the best solution to obtain the current best solution (global solution). The exploitation phase of MRFO technique is a poor operator as it is not dependent on the fitness of current solution. In the modified MRFO algorithm, this operator is improved using an efficient local search (SA algorithm) which explores new neighboring solutions to obtain the best global solutions. The

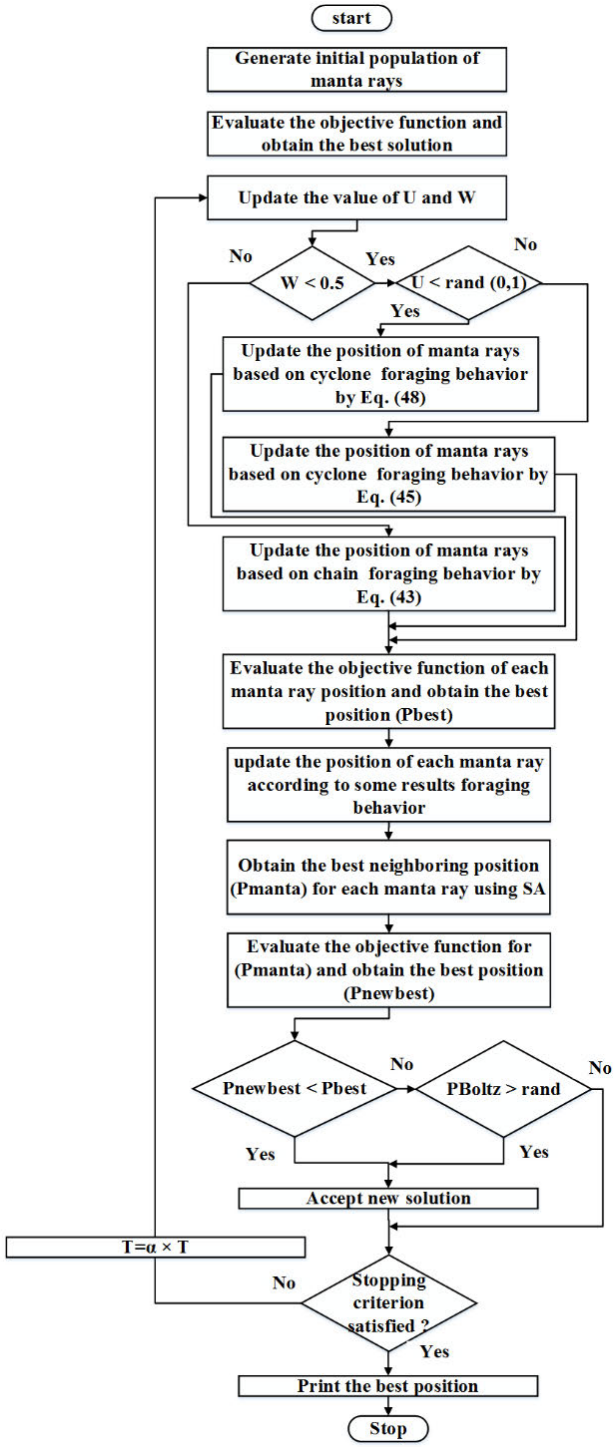

FIGURE 6. Modified MRFO algorithm flowchart.

steps of the modified MRFO technique for obtaining the optimal allocation of WT and PV without/with BESS in RDS are summarized as follows:

Step 1: Generate the first value of agents among the lower and upper value of variables as shown next.

$$P_i^d(z) = LP^d + rand(UP^d - LP^d) \tag{56}$$

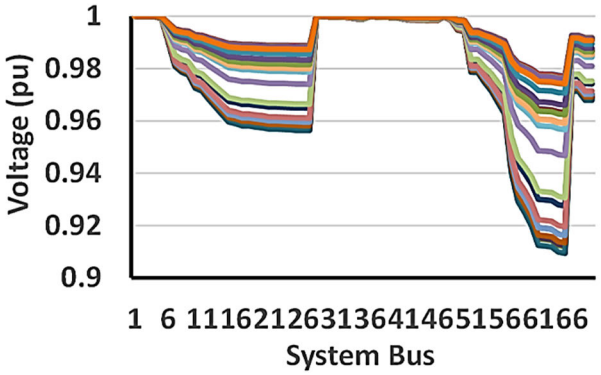

FIGURE 7. Bus system voltages during the day without RES.

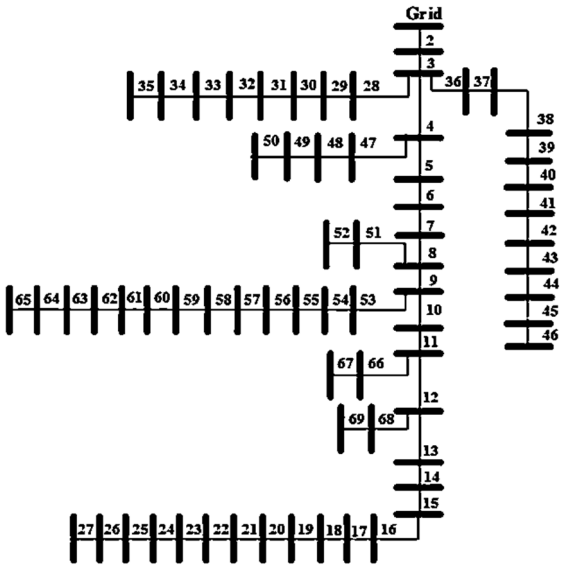

FIGURE 8. IEEE 69-bus RDS.

Step 2: Calculate the fitness for each position agent and get the superior position.

Step 3: Update the value of U and W as follows:

$$U = \frac{Current\ iteration}{Maximum\ iteration}, \quad W = random(0, 1)$$

Step 4: If $W < 0.5$ and $U <$ rand (0, 1), the updating positions of agents are calculated by (54).

Step 5: If $W < 0.5$ and $U \geq$ rand (0, 1), the updating positions of agents are calculated by (51).

Step 6: If $W > 0.5$, the updating positions of agent can be evaluated by (49).

Step 7: Evaluate the fitness for each position of agents and get the superior position.

Step 8: Evaluate the positions of agents by (55).

Step 9: Obtain the neighboring position for each position of the agent using SA.

Step 10: Calculate the fitness for each position of the agents and get the superior position.

Step 11: When the stopping criterion isn't satisfied, return to Step 3.

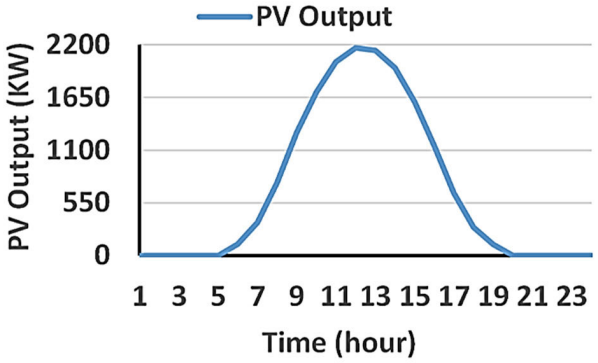

FIGURE 9. Output power of PV during the day by installing 1-PV alone in RDS.

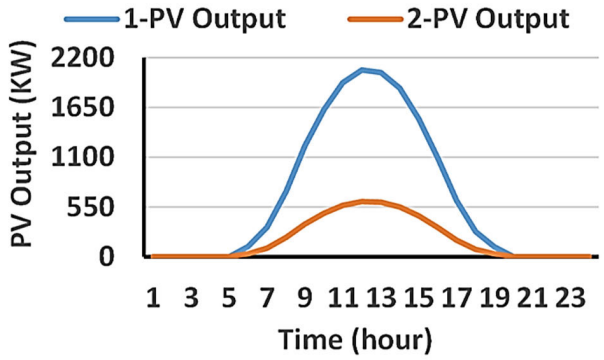

FIGURE 10. Output of PV during the day by installing 2-PV alone in RDS.

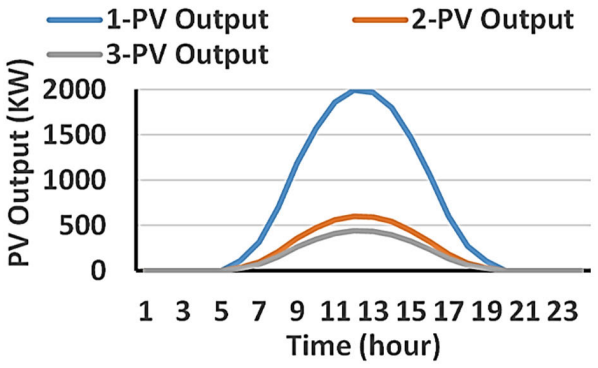

FIGURE 11. Output of PV during the day by installing 3-PV alone in RDS.

Step 12: Get the superior solutions (best sizes and positions of WT, PV, and BESS).

VII. SIMULATION RESULTS

In this section, the standard IEEE 69-bus RDS, shown in Fig. 8, is utilized to measure the performance of the proposed MRFO. This test system includes load demand of 2.695 MVar and 3.802 MW with sixty-nine buses and sixty-eight branches [57]. The system base values are 12.66 kV and 10 MVA. The reactive and active losses of RDS

TABLE 1. The used parameters.

Item	Value
Agent number	30
Maximum iteration	2000
Voltage constraints	$0.90 \leq V_j \leq 1.05$
sizing constraints P_{WT}	$0\ \text{kW} \leq P_{WT} \leq 4000\ \text{kW}$
sizing limits P_{PV}	$0\ \text{kW} \leq P_{PV} \leq 4000\ \text{kW}$
Percentage of Stored energy per total capacity of BESS unit	$20\% \leq E_{BES,j}(t) \leq 90\%$

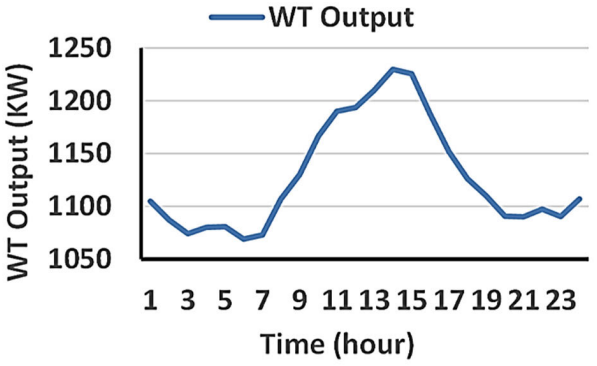

FIGURE 12. Output of WT during the day by installing 1-WT alone in RDS.

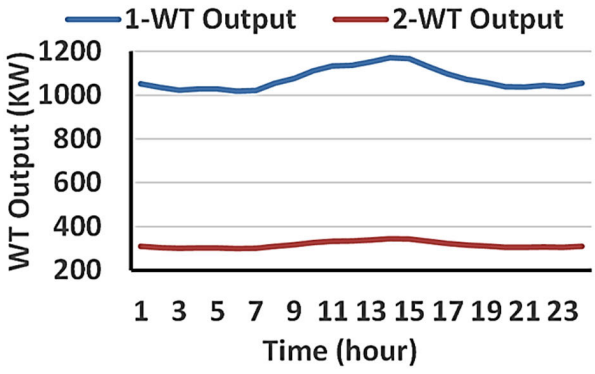

FIGURE 13. Output of WT during the day by installing 2-WT alone in RDS.

without installation of WT, PV, and BESS, are 989.233 KVar and 2173.851 kW, respectively. The following results are obtained by MATLAB R2019b. The parameters of the PV module are $V_{oc} = 36.96$V, $I_{sc} = 8.38$A, V_MPP = 28.36V, I_MPP = 7.76A, $K_v = 0.1278$V/°C and $K_i = 0.00545$A/°C. The round-trip efficiency of the BESS is 77%. TABLE 1 includes the used parameters.

To measure the efficiency of the presented technique, the following cases are studied:

A. CASE 1. BASE CASE (WITHOUT INSTALLATION OF RES)

The simulation results in the base case are obtained without any installation for PV or WT in the RDS. In this case, the minimum voltage in the RDS at bus 65 is 0.909 p.u. and the total system loss is 2173.851 kW, as shown in Fig.7.

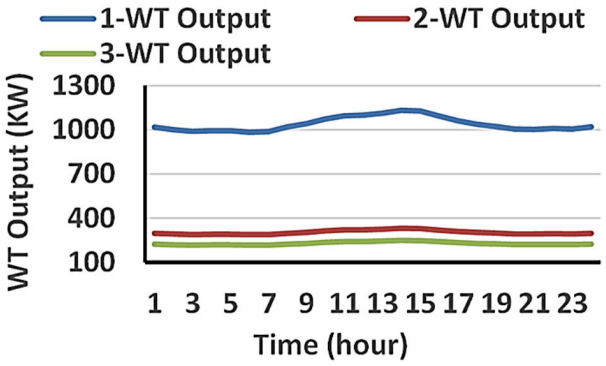

FIGURE 14. Output of WT during the day by installing 3-WT alone in RDS.

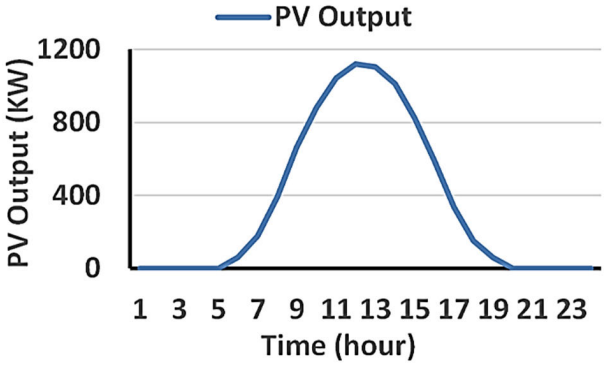

FIGURE 15. Output of PV during the day by installing 1-PV and 1-WT without BESS in RDS.

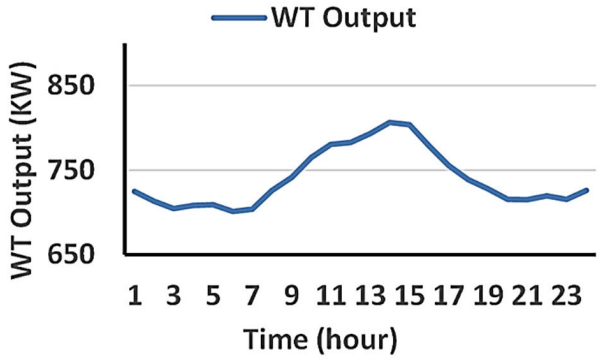

FIGURE 16. Output of WT during the day by installing 1-PV and 1-WT in RDS.

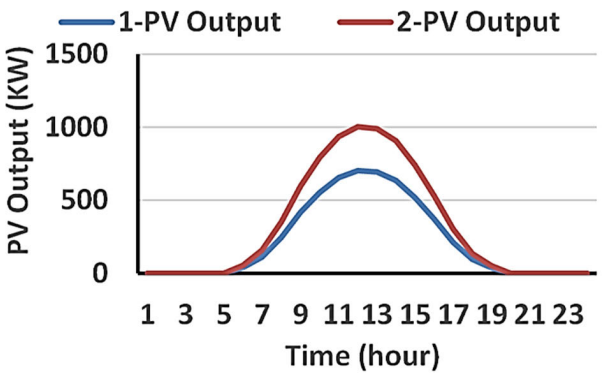

FIGURE 17. Output of PV during the day by installing 2-PV and 2-WT without BESS in RDS.

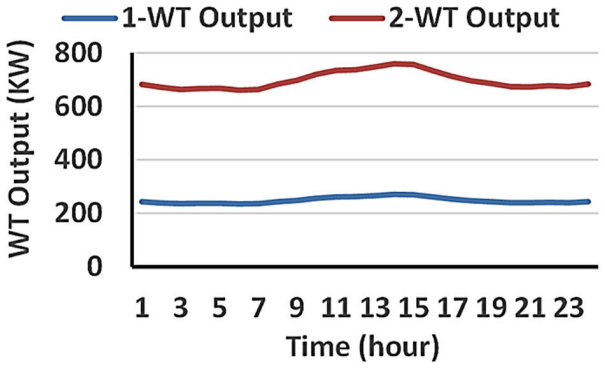

FIGURE 18. Output of PV during the day by installing 2-PV and 2-WT without BESS in RDS.

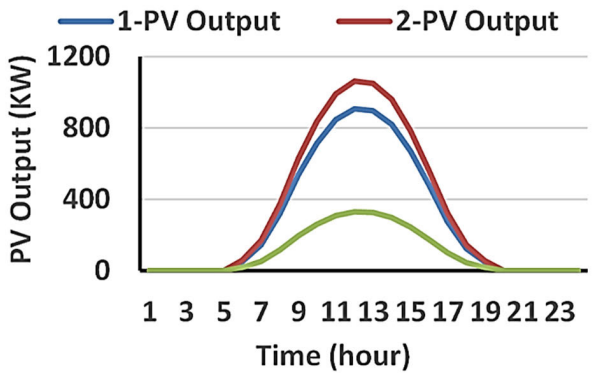

FIGURE 19. Output of PV during the day by installing 3-PV and 3-WT without BESS in RDS.

B. CASE 2. INSTALLATION OF PV IN RDS

In this case, the PV is integrated in RDS to inject active power only, meaning that the inverter based PV operates at unity power factor. The optimal sizes and locations of the PV in the case of one, two, and three units are given in TABLE 2. In the case of allocating one PV unit in RDS, the optimal PV size and location are 2168.238 kW at bus 61. When allocating two PV units, the optimal PV sizes and locations are 2063.052 kW at bus 61 and 611.57 kW at bus 17. Finally, when installing three PV units, the optimal PV sizes are 1991.45 kW, 439.53 kW, and 599.51 kW and the best positions are at bus 61, bus17, and bus 11, respectively. The total active losses are decreased to 1124.54 kW, 1038.229 kW, and 1021.694 kW when installing one, two, and three PV units, respectively. The generated power by the PV units during the day are shown in Figures 9-11. The energy during the day for one PV unit is 16319 kWh at bus 61 and for two PV units are 15527 kWh at bus 61 and 4603 kWh at bus 17. Also,

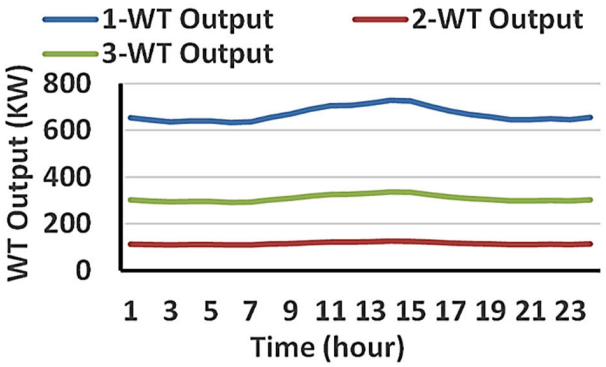

FIGURE 20. Output of WT during the day by installing 3-PV and 3-WT without BESS in RDS.

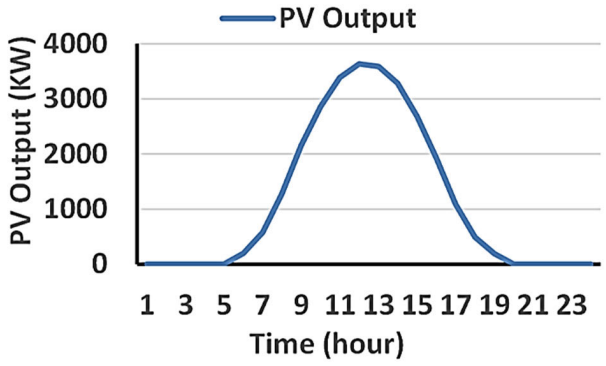

FIGURE 21. Output of PV during the day by installing 1-(PV+BESS) and WT in RDS.

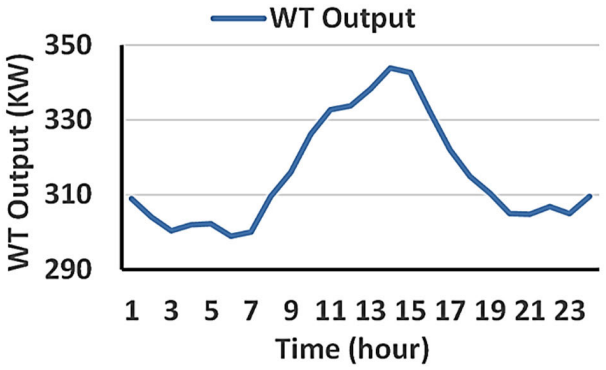

FIGURE 22. Output of WT during the day by installing 1-(PV+BESS) and WT in RDS.

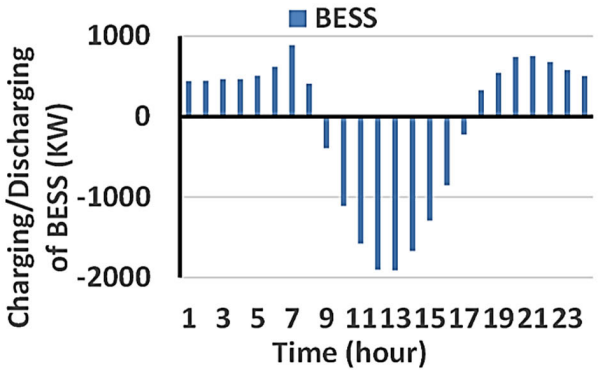

FIGURE 23. Charging and discharging of 1-BESS during the day by installing 1-(PV+BESS) and WT in RDS.

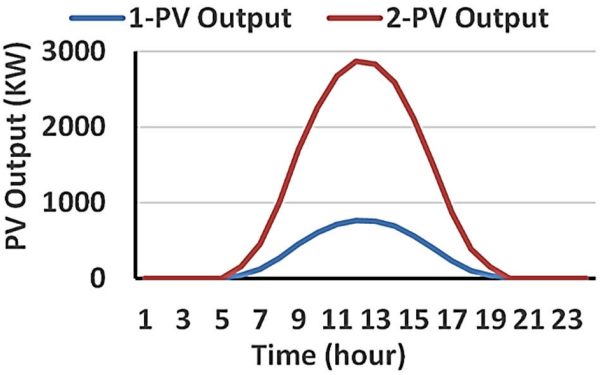

FIGURE 24. Output of PV during the day by installing 2-(PV+BESS) and WT in RDS.

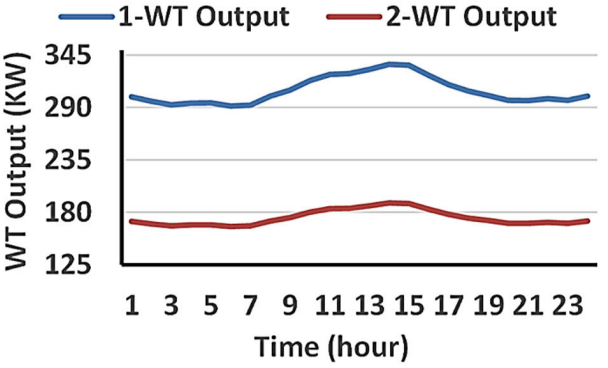

FIGURE 25. Output of WT during the day by installing 2-(PV+BESS) and WT in RDS.

the energy during the day for three PV units are 14989 kWh at bus 61, 4512.1 kWh at bus 11 and 3308.1 kWh at bus 17. By allocating PV in the RDS, the minimum voltage at bus 65 is improved from 0.909 p.u to 0.9407 p.u., as presented in TABLE 2.

C. CASE 3. INSTALLATION OF WT IN RDS

In this case, the WT is allocated in the distribution network to supply active power, during the day, without reactive power capability of the inverter. The best locations and sizes of WT units are presented in TABLE 2. When one WT unit is installed, the optimal size and location are 2051.9 kW at bus 61, respectively. In this case, the minimum voltage is improved to 0.9549 p.u, By integrating two WT units, the optimal sizes are 1954.23 kW at bus of 61 and 573.8 kW at bus of 17, while the power loss is reduced to 920.147 kW. By installing three WT units, the optimal sizes are 1888.498 kW, 552.113 kW, and 415.747 kW at buses

TABLE 2. The obtained results for integrating PV alone, WT alone, and simultaneous WT and PV without BESS in RDS.

Item	Bus (PV size (KW))	Bus (WT size (KW))	P_{loss} (KW)	Bus (Minimum Voltage)	Bus (Maximum Voltage)	Maximum Voltage of $Bus_{(PV)}$	Maximum Voltage of $Bus_{(WT)}$
Without PV and WT	-	-	2173.8506	65(0.9093)	2(1.0000)	-	-
1-PV alone	61(2168.238)	-	1124.54	65(0.9407)	2(1.0000)	61(0.9967)	-
2-PV alone	61(2063.052) 17(611.57)	-	1038.229	65(0.9407)	2(1.0000)	61(0.9968) 17(0.9982)	-
3-PV alone	61(1991.45) 17(439.53) 11(599.51)	-	1021.694	65(0.9407)	2(1.0000)	61(0.9968) 17(0.9983) 11(0.9981)	-
1-WT alone	-	61(2051.9)	1015.892	65(0.9549)	61(1.0154)	-	61(1.0154)
2-WT alone	-	61(1954.23) 17(573.8)	920.147	65(0.9549)	61(1.0154)	-	61(1.0154)
3-WT alone	-	61(1888.498) 11(552.113) 17(415.747)	902.379	65(0.9549)	61(1.0155)	-	61(1.0155)
1- WT and PV	62(1118.95)	61(1345.58)	875.069	65(0.9589)	61(1.0029)	62(1.0028)	61(1.0029)
2- WT and PV	62(1003.655) 11(702.779)	61(1267.06) 17(450.948)	751.632	65(0.9589)	61(1.0029)	62(1.0028) 11(0.9996)	61(1.0029) 17(1.0028)
3- WT and PV	62(1063.331) 49(908.577) 17(330.418)	61(1214.872) 21(209.2) 11(560.32)	735.342	65(0.9589)	61(1.0029)	62(1.0028) 49(0.9986) 17(1.0011)	61(1.0029) 21(1.0014) 11(1.0015)

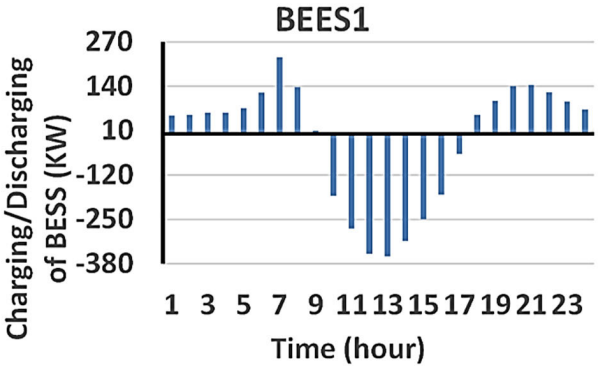

FIGURE 26. Discharging and charging of BESS#1 during the day by installing 2-(PV+BESS) and WT in RDS.

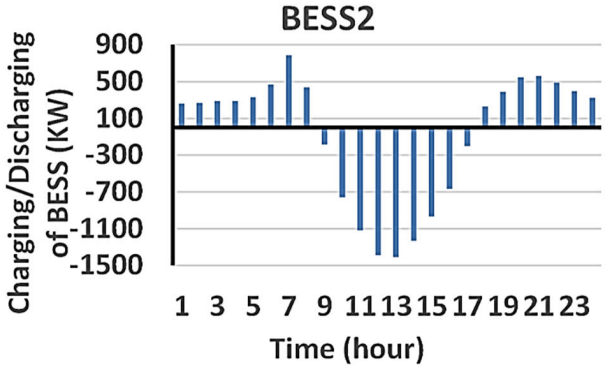

FIGURE 27. Discharging and charging of BESS#2 during the day by installing 2-(PV+BESS) and WT in RDS.

of 61, 11, and 17, respectively. The power loss in this case is reduced to 902.379 kW. Figure 12 shows that the generated energy by one WT unit during the day is 27073kWh at bus 61. Also, the total energy during the day for two WT are 25784 kWh at bus 61 and 7570.8 kWh at bus 17 as shown in Figure 13. The injection energy of three WT units to the system during the day are 24917 kWh at bus 61, 7284.6 kWh at bus 11 and 5485.4 kWh at bus 17 as shown in Figure 14.

D. CASE 4. INSTALLATION OF WT AND PV IN RDS

In this case, the installation of WT and PV at the best locations in RDS is studied. This case is divided into the following two subcases.

1) INSTALLATION OF WT AND PV WITHOUT BESS IN RDS

In this case, both WT and PV are installed in the RDS to inject active power only. TABLE 2 illustrates the best locations and sizes of WT and PV. From TABLE 2, it can be observed that the integration of one unit of WT and PV improves the minimum voltage profile at bus 65 to 0.9589 p.u and reduces the system loss to 875.069 kW. Also, the power loss is reduced to 735.342 kW and 751.632 kW by integrating three and two of WT and PV, respectively. From Figure 15, one PV generates total energy of 8421.8 kWh at bus 62 to the grid during the day. Also, one WT generates total energy of 17754 kWh at bus 61 as shown in Figure 16. The total energies for two PV units during the day are 5289.4 kWh at bus 11 and 7554 kWh at bus 62 as shown in Figure 17. Also, the total energies for two WT during the day are 5949.8 kWh at bus 17 and 16718 kWh at bus 61 as shown in Figure 18. From Figure 19, the total energies during the day for three PV are 6838.4 kWh, 8003.1 kWh and 2486.9 kWh at buses 49, 62 and 17, respectively. Also, the total energies during the day for three WT units are 16029 kWh, 2760.2 kWh and 7392.9 kWh at buses 61, 21 and 11, respectively as shown in Figure 20. It is worth mentioning that the installing three

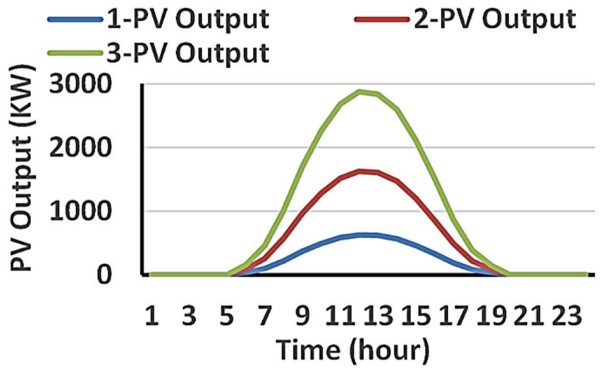

FIGURE 28. Output of PV during the day by installing 3-(PV+BESS) and WT in RDS.

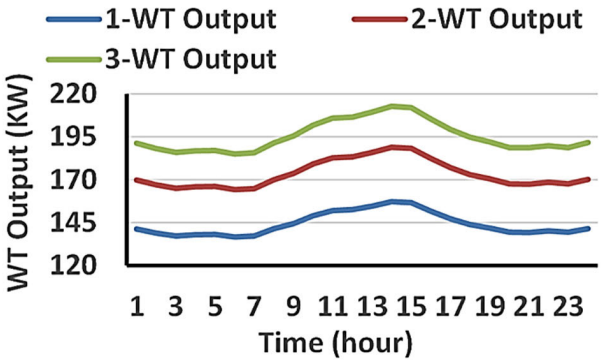

FIGURE 29. Output of WT during the day by installing 3-(PV+BESS) and WT in RDS.

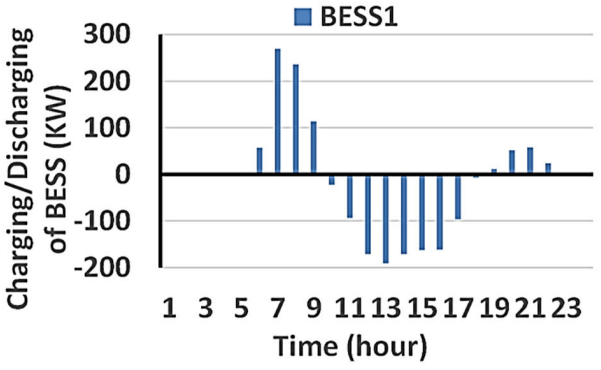

FIGURE 30. Discharging and charging of BESS#1 during the day by installing 3-(PV+BESS) and WT in RDS.

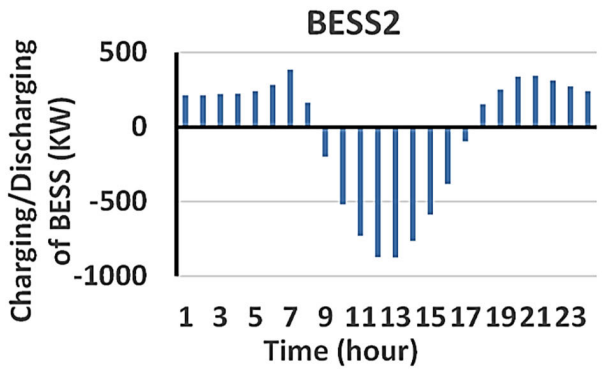

FIGURE 31. Discharging and charging of BESS#2 during the day by installing 3-(PV+ BESS) and WT in RDS.

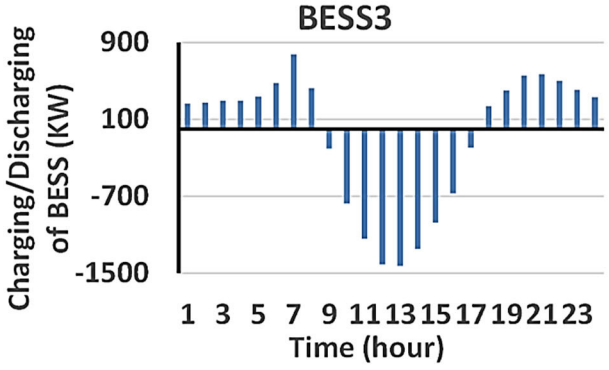

FIGURE 32. Discharging and charging of BESS#3 during the day by installing 3-(PV+BESS) and WT in RDS.

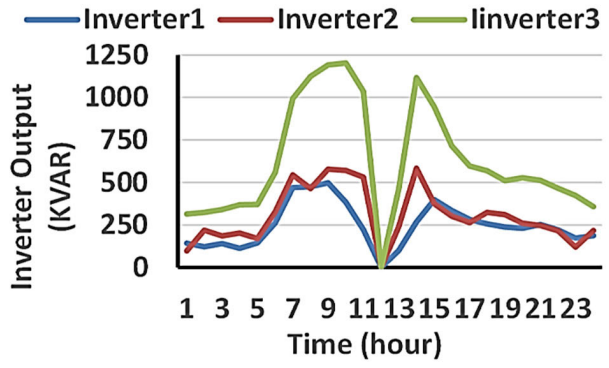

FIGURE 33. Injected reactive power of PV inverters during the day by installing three (PV+BESS) and WT in RDS.

units of WT and PV significantly decreases the system loss, and it gives better results than the integration of one and two combinations of PV and WT units.

2) INSTALLATION OF WT AND PV WITH BESS IN RDS

In this case, the BESS is used with the PV. Both WT and the combination of PV and BESS are optimally installed in the RDS to generate active power only. Integration of three, two, and one of WT and (PV+BESS) units decrease the system power loss to 672.575 kW, 687.184 kW, and 727.261 kW, respectively, as shown in TABLE 3. Compared to TABLE 2, integration of BESS with PV at the same location achieves best solutions than incorporating PV without BESS in the RDS. The optimal size and allocation of one WT and (PV+BESS) are 573.716 kW for WT at bus 17, 3633.24 kW for PV at bus 61, and 1909.128 kW for BESS at bus 61. The power generation of the PV, WT, and BESS in case of using one unit of (PV+BESS) and WT are

TABLE 3. Obtained results for integrating WT and (PV+BESS) with and without enabling PV inverter in RDS.

Item	Bus (PV size (KW))	Bus (BESS size (KW))	Bus (inverter size (KVARh))	Bus (WT size (KW))	P_{loss} (KW) Without inverter	Ploss(KW) With inverter	$E_{charging}$ (KWh)	$E_{discharging}$ (KWh)	E_{PV} (KWh)	$E_{PV\ to\ grid}$ (KWh)
1-WT and (PV+BESS)	61(3633.24)	61(1909.128)	-	17(573.7155)	727.2614	-	10925.8	8353.73	61(27345.412)	61(16419.631)
2- WT and (PV+BESS)	17(766.5307) 61(2869.1199)	17(358.5995) 61(1407.5087)	-	11(559.3022) 64(316.6494)	687.1835	-	17(2005.074) 61(7927.247)	17(1533.057) 61(6061.085)	17(5769.26) 61(21594.29)	17(3764.182) 61(13667.045)
3- WT and (PV+BESS)	12(628.814) 49(1630.481) 61(2875.938)	12(191.576) 49(875.064) 61(1424.417)	1(5.919)2 4(7.3559 (15.025) 61	11(262.22) 64(315.26) 17(355.13)	672.575	117.5597	12(1083.691) 49(5028.758) 61(8034.982)	12(825) 49(3844.933) 61(6143.458)	12(4732.735) 49(12271.74) 61(21645.61)	12(3649.044) 49(7242.978) 61(13610.63)

illustrated in Figures 21, 22, and 23, respectively. The best location and sizing of WT in case of using two units of WT and (PV+BESS) are 559.302 kW and 316.649 kW at buses 11 and 64, respectively. The best sizes of (PV+BESS) in case of using two units of WT and (PV+BESS) are 766.531 kW and 2869.12 kW for PV, 358.6 kW and 1407.509 kW for BESS at buses 17 and 61, respectively. The output power of the PV, WT, and BESS for two units of WT and (PV+BESS) are shown in Figures 24 to 27, respectively. The best sizes of (PV+BESS) for three WT and (PV+BESS) are 628.814 kW, 1630.481kW, 2875.938KW for PV, and 191.576 kW, 875.064 kW, and 1424.417 kW for BESS at buses 12, 49, and 61, respectively. Further, the optimal allocation of WT for three WT and (PV+BESS) are 262.22 kW, 315.26 kW and 355.13 kW at buses 11, 64, and 17, respectively. The power generation of the WT, PV, and BESS for three WT and (PV+BESS) are shown in Figures 28-32.

The charging and discharging energies of one BESS for one WT and (PV+BESS) are 10925.8 kWh and 8353.73 kWh, respectively, while the injected energy from the PV into the grid is 16419.631 kWh. By installing two PV and WT in the RDS, 1533.057 kWh and 6061.085 kWh are injected by the BESS, and 3764.182 kWh and 13667.045 kWh are injected by the PV at buses 17 and 61, respectively, as given in TABLE 3. The charging energies of the two BESS for two WT and (PV+BESS) are 2005.074 kWh and 7927.247 kWh, while the total output energy from the two PV units are 5769.26 kWh and 21594.29 kWh at buses 17 and 61, respectively. Moreover, the integration of three WT and PV in the RDS leads to inject 3649.044 kWh, 7242.978 kWh, and 13610.63 kWh from the PV and inject 825 kWh, 3844.933 kWh, and 6143.458 kWh from the BESS at buses 12, 49 and 61, respectively.

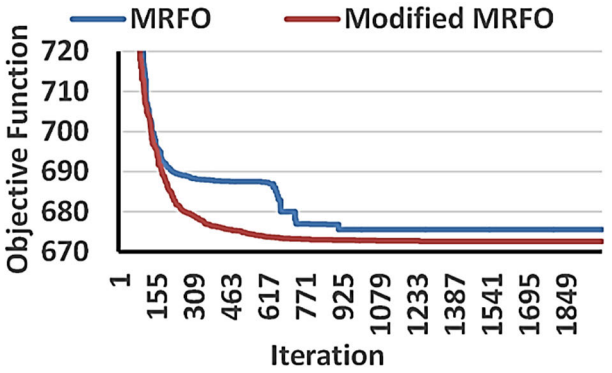

FIGURE 34. Convergence characteristics of modified MRFO and original MRFO algorithms for installing three (PV+BESS) and WT in RDS.

From Figures 30 to 32, the charging energy of BESS for the three WT and PV with BESS are 1083.691 kWh, 5028.758 kWh, and 8034.982 kWh at buses 12, 49, and 61, respectively. The best case of all previous cases is the three WT and (PV+BESS). Therefore, next we study the effect of enabling the reactive power by the PV inverter on system performance considering this case. The location of the interfacing inverter is the same as the location of PV and BESS. The integration of three WT and (PV+BESS) considering reactive power by the PV inverters, reduces the system losses until 117.56 kW and improves the minimum bus voltage at bus 65 to 0.981 p.u. Fig. 33 shows the reactive power absorbed/injected by the PV inverters during the day. From Figure 33, the total reactive energies during the day for three PV inverters of three WT and (PV+BESS) units are 5918.5 kVArh, 7354.7 kVArh and 15025 kVArh at buses 12, 49 and 61, respectively. The maximum reactive power

TABLE 4. Obtained results for integrating WT and (PV+BESS) without enabling PV inverter in RDS by MMRFO and MRFO algorithms.

Item		Location (PV size)	Location (WT size)	Location (BESS size)	P_{loss} (KW)
Modified MRFO algorithm	1	61(3633.24)	17(573.7155)	61(1909.128)	727.2614
	2	17(766.5307) 61(2869.1199)	11(559.3022) 64(316.6494)	17(358.5995) 61(1407.5087)	687.1835
	3	12(628.814) 49(1630.481) 61(2875.938)	11(262.22) 64(315.26) 17(355.13)	12(191.576) 49(875.064) 61(1424.417)	672.575
MRFO algorithm	1	61(3633.24)	17(573.7155)	61(1909.128)	727.2614
	2	17(817.5495) 61(2520.9587)	11(546.22) 64(467.2631)	17(414.730) 61(1166.6662)	688.876
	3	12(858.7037) 49(1735) 61(2575.1)	11(167.9923) 64(445.1928) 17(333.3840)	12(385.3934) 49(1036.9946) 61(1201.19)	675.5705

TABLE 5. The statistical results and simulation time of Modified MRFO algorithm and MRFO algorithm for integrating WT and (PV+BESS) in RDS.

Item		Minimum	Average	Maximum	STD	Simulation Time of Minimum Value (second)
Modified MRFO algorithm	1	727.2614	727.2614	727.2615	4.4721E-05	2216.76516
	2	687.1835	688.2110	689.2807	0.8121	2611.97612
	3	672.5753	676.0891	678.437	2.3567	2678.18284
MRFO algorithm	1	727.2614	727.2616	727.2620	2.5495E-04	1910.78880
	2	688.8760	697.1332	713.9421	10.5251	2501.49259
	3	675.5705	694.2808	721.4942	22.2950	2566.97361

of three PV inverters are 498.036 kVAr at nine o'clock, 583.896 kVAr at fourteen o'clock and 1203 kVAr at ten o'clock at buses 12, 49 and 61. These results demonstrate that enabling the reactive power capability of the PV inverters has a significant effect on voltage profiles and system loss reduction in distribution systems. Fig. 34 and TABLE 4 show that the modified MRFO can obtain the best global results of three WT and (PV+BESS) with fewer iterations compared with the original MRFO algorithm. TABLE 5 shows the statistical results of MRFO and modified MRFO algorithms for integrating one, two and three of WT and PV with BESS in RDS. The modified MRFO algorithm obtains the global results with high simulation time compared to MRFO algorithm as shown in TABLE 5. The reason is that the modified MRFO algorithm consists of MRFO algorithm to obtain the initial best results and SA algorithm to obtain the best neighboring results by searching around the initial best results of MRFO algorithm. Therefore, the simulation time of the modified MRFO algorithm is the summation of simulation time for both MRFO and SA algorithms together.

VIII. CONCLUSION

In this paper, a modified MRFO algorithm has been developed and applied to determine the optimal allocation of WT and PV units without/with BESS in RDS. This proposed algorithm is based on the MRFO algorithm, representing the exploration phase, and SA algorithm which enhances the exploitation phase of the original MRFO. To reduce the search space, QLSF has been utilized to obtain the best candidate buses for installing WT, PV, and BESS in RDS. The obtained results achieved maximum reduction in total active power losses as a single objective function. The simulation results have been obtained using the modified algorithm considering a time-varying load demand and the stochastic nature of PV and WT generation. The integration of multiple PV and WT gives better results than integrating one PV and WT in RDS. Also, integration of WT and (PV+BESS) in the RDS leads to lower system power losses than the integration of WT and PV individually. In the case of three units of WT and (PV+BESS), enabling reactive power capability of the PV inverters, the system power losses significantly reduced compared with other cases. Regarding the convergence characteristics, the modified algorithm gives the global best results with fewer number of iterations than the original algorithm. The obtained results proved that the modified algorithm is efficient to be used in complex and challenging optimization engineering problems and can escape from the local solution to the global solution.

ACKNOWLEDGEMENT

The authors thank the support of the National Research and Development Agency of Chile (ANID), ANID/Fondap/15110019.

REFERENCES

[1] M. Ashari and C. V. Nayar, "An optimum dispatch strategy using set points for a photovoltaic (PV)–diesel–battery hybrid power system," *Solar Energy*, vol. 66, no. 1, pp. 1–9, 1999.
[2] S. Rehman and L. M. Al-Hadhrami, "Study of a solar PV–diesel–battery hybrid power system for a remotely located population near Rafha, Saudi Arabia," *Energy*, vol. 35, no. 12, pp. 4986–4995, Dec. 2010.
[3] M. A. M. Ramli, H. R. E. H. Bouchekara, and A. S. Alghamdi, "Optimal sizing of PV/wind/diesel hybrid microgrid system using multi-objective self-adaptive differential evolution algorithm," *Renew. Energy*, vol. 121, pp. 400–411, Jun. 2018.
[4] R. H. A. Zubo, G. Mokryani, H.-S. Rajamani, J. Aghaei, T. Niknam, and P. Pillai, "Operation and planning of distribution networks with integration of renewable distributed generators considering uncertainties: A review," *Renew. Sustain. Energy Rev.*, vol. 72, pp. 1177–1198, May 2017.
[5] D. C. Momete, "Analysis of the potential of clean energy deployment in the European Union," *IEEE Access*, vol. 6, pp. 54811–54822, 2018.

[6] H. Lucas, S. Pinnington, and L. F. Cabeza, "Education and training gaps in the renewable energy sector," *Solar Energy*, vol. 173, pp. 449–455, Oct. 2018.
[7] P. Trop and D. Goricanec, "Comparisons between energy carriers' productions for exploiting renewable energy sources," *Energy*, vol. 108, pp. 155–161, Aug. 2016.
[8] Z. Abdmouleh, A. Gastli, L. Ben-Brahim, M. Haouari, and N. A. Al-Emadi, "Review of optimization techniques applied for the integration of distributed generation from renewable energy sources," *Renew. Energy*, vol. 113, pp. 266–280, Dec. 2017.
[9] S. Mekhilef, R. Saidur, and M. Kamalisarvestani, "Effect of dust, humidity and air velocity on efficiency of photovoltaic cells," *Renew. Sustain. Energy Rev.*, vol. 16, no. 5, pp. 2920–2925, Jun. 2012.
[10] F. Rizzi, N. J. van Eck, and M. Frey, "The production of scientific knowledge on renewable energies: Worldwide trends, dynamics and challenges and implications for management," *Renew. Energy*, vol. 62, pp. 657–671, Feb. 2014.
[11] J. Paska, P. Biczel, and M. Kłos, "Hybrid power systems—An effective way of utilising primary energy sources," *Renew. Energy*, vol. 34, no. 11, pp. 2414–2421, Nov. 2009.
[12] A. Raheem, S. A. Abbasi, A. Memon, S. R. Samo, Y. H. Taufiq-Yap, M. K. Danquah, and R. Harun, "Renewable energy deployment to combat energy crisis in Pakistan," *Energy, Sustainability Soc.*, vol. 6, no. 1, pp. 1–13, Dec. 2016.
[13] A. Ashfaq and A. Ianakiev, "Features of fully integrated renewable energy atlas for Pakistan; wind, solar and cooling," *Renew. Sustain. Energy Rev.*, vol. 97, pp. 14–27, Dec. 2018.
[14] N. A. Ludin, N. I. Mustafa, M. M. Hanafiah, M. A. Ibrahim, M. A. M. Teridi, S. Sepeai, A. Zaharim, and K. Sopian, "Prospects of life cycle assessment of renewable energy from solar photovoltaic technologies: A review," *Renew. Sustain. Energy Rev.*, vol. 96, pp. 11–28, Nov. 2018.
[15] F. Dinçer, "The analysis on photovoltaic electricity generation status, potential and policies of the leading countries in solar energy," *Renew. Sustain. Energy Rev.*, vol. 15, no. 1, pp. 713–720, Jan. 2011.
[16] F. Liu, R. Li, Y. Li, R. Yan, and T. Saha, "Takagi–Sugeno fuzzy model-based approach considering multiple weather factors for the photovoltaic power short-term forecasting," *IET Renew. Power Gener.*, vol. 11, no. 10, pp. 1281–1287, Aug. 2017.
[17] M. Rizwan, G. Mujtaba, S. A. Memon, K. Lee, and N. Rashid, "Exploring the potential of microalgae for new biotechnology applications and beyond: A review," *Renew. Sustain. Energy Rev.*, vol. 92, pp. 394–404, Sep. 2018.
[18] M. Yang and X. Huang, "Ultra-short-term prediction of photovoltaic power based on periodic extraction of PV energy and LSH algorithm," *IEEE Access*, vol. 6, pp. 51200–51205, Sep. 2018.
[19] A. A. K. Arani, G. B. Gharehpetian, and M. Abedi, "Review on energy storage systems control methods in microgrids," *Int. J. Electr. Power Energy Syst.*, vol. 107, pp. 745–757, May 2019.
[20] Y. M. Atwa and E. F. El-Saadany, "Optimal allocation of ESS in distribution systems with a high penetration of wind energy," *IEEE Trans. Power Syst.*, vol. 25, no. 4, pp. 1815–1822, Nov. 2010.
[21] J. Ahmad, M. Imran, A. Khalid, W. Iqbal, S. R. Ashraf, M. Adnan, S. F. Ali, and K. S. Khokhar, "Techno economic analysis of a wind-photovoltaic-biomass hybrid renewable energy system for rural electrification: A case study of Kallar Kahar," *Energy*, vol. 148, pp. 208–234, Apr. 2018.
[22] A. Maleki and A. Askarzadeh, "Optimal sizing of a PV/wind/diesel system with battery storage for electrification to an off-grid remote region: A case study of Rafsanjan, Iran," *Sustain. Energy Technol. Assessments*, vol. 7, pp. 147–153, Sep. 2014.
[23] M. J. Khan, A. K. Yadav, and L. Mathew, "Techno economic feasibility analysis of different combinations of PV-wind-diesel-battery hybrid system for telecommunication applications in different cities of Punjab, India," *Renew. Sustain. Energy Rev.*, vol. 76, pp. 577–607, Sep. 2017.
[24] M. Hossain, S. Mekhilef, and L. Olatomiwa, "Performance evaluation of a stand-alone PV-wind-diesel-battery hybrid system feasible for a large resort center in South China Sea, Malaysia," *Sustain. Cities Soc.*, vol. 28, pp. 358–366, Jan. 2017.
[25] M. Arbabzadeh, J. X. Johnson, G. A. Keoleian, P. G. Rasmussen, and L. T. Thompson, "Twelve principles for green energy storage in grid applications," *Environ. Sci. Technol.*, vol. 50, no. 2, pp. 1046–1055, Jan. 2016.
[26] J. P. Barton and D. G. Infield, "Energy storage and its use with intermittent renewable energy," *IEEE Trans. Energy Convers.*, vol. 19, no. 2, pp. 441–448, Jun. 2004.
[27] H. Bevrani, A. Ghosh, and G. Ledwich, "Renewable energy sources and frequency regulation: Survey and new perspectives," *IET Renew. Power Gener.*, vol. 4, no. 5, pp. 438–457, Sep. 2010.
[28] A. R. Abul'Wafa, "Optimization of economic/emission load dispatch for hybrid generating systems using controlled elitist NSGA-II," *Electr. Power Syst. Res.*, vol. 105, pp. 142–151, Dec. 2013.
[29] D. Q. Hung, N. Mithulananthan, and R. C. Bansal, "Integration of PV and BES units in commercial distribution systems considering energy loss and voltage stability," *Appl. Energy*, vol. 113, pp. 1162–1170, Jan. 2014.
[30] M. F. Zia, E. Elbouchikhi, and M. Benbouzid, "Microgrids energy management systems: A critical review on methods, solutions, and prospects," *Appl. Energy*, vol. 222, pp. 1033–1055, Jul. 2018.
[31] S. M. Dawoud, X. Lin, and M. I. Okba, "Hybrid renewable microgrid optimization techniques: A review," *Renew. Sustain. Energy Rev.*, vol. 82, pp. 2039–2052, Feb. 2018.
[32] R. Siddaiah and R. P. Saini, "A review on planning, configurations, modeling and optimization techniques of hybrid renewable energy systems for off grid applications," *Renew. Sustain. Energy Rev.*, vol. 58, pp. 376–396, May 2016.
[33] R. Chedid and A. Sawwas, "Optimal placement and sizing of photovoltaics and battery storage in distribution networks," *Energy Storage*, vol. 1, no. 4, p. 46, Aug. 2019.
[34] J.-H. Teng, S.-W. Luan, D.-J. Lee, and Y.-Q. Huang, "Optimal charging/discharging scheduling of battery storage systems for distribution systems interconnected with sizeable PV generation systems," *IEEE Trans. Power Syst.*, vol. 28, no. 2, pp. 1425–1433, May 2013.
[35] A. Nottrott, J. Kleissl, and B. Washom, "Energy dispatch schedule optimization and cost benefit analysis for grid-connected, photovoltaic-battery storage systems," *Renew. Energy*, vol. 55, pp. 230–240, Jul. 2013.
[36] K. Kasturi and M. R. Nayak, "Optimal planning of charging station for EVs with PV-BES unit in distribution system using WOA," in *Proc. 2nd Int. Conf. Man Mach. Interfacing (MAMI)*, Dec. 2017, pp. 1–6.
[37] L. A. Wong, V. K. Ramachandaramurthy, S. L. Walker, P. Taylor, and M. J. Sanjari, "Optimal placement and sizing of battery energy storage system for losses reduction using whale optimization algorithm," *J. Energy Storage*, vol. 26, Dec. 2019, Art. no. 100892.
[38] H. Abdel-Mawgoud, S. Kamel, M. Khasanov, and T. Khurshaid, "A strategy for PV and BESS allocation considering uncertainty based on a modified Henry gas solubility optimizer," *Electr. Power Syst. Res.*, vol. 191, Feb. 2021, Art. no. 106886.
[39] V. Kalkhambkar, R. Kumar, and R. Bhakar, "Joint optimal sizing and placement of renewable distributed generation and energy storage for energy loss minimization," in *Proc. 4th Int. Conf. Adv. Comput. Commun. Syst. (ICACCS)*, Jan. 2017, pp. 1–9.
[40] A. Fathy and A. Y. Abdelaziz, "Grey wolf optimizer for optimal sizing and siting of energy storage system in electric distribution network," *Electr. Power Compon. Syst.*, vol. 45, no. 6, pp. 601–614, Apr. 2017.
[41] M. R. Elkadeem, M. A. Elaziz, Z. Ullah, S. Wang, and S. W. Sharshir, "Optimal planning of renewable energy-integrated distribution system considering uncertainties," *IEEE Access*, vol. 7, pp. 164887–164907, 2019.
[42] H. Saboori, R. Hemmati, and M. A. Jirdehi, "Reliability improvement in radial electrical distribution network by optimal planning of energy storage systems," *Energy*, vol. 93, pp. 2299–2312, Dec. 2015.
[43] A. Ali, K. Mahmoud, D. Raisz, and M. Lehtonen, "Optimal allocation of inverter-based WTGS complying with their DSTATCOM functionality and PEV requirements," *IEEE Trans. Veh. Technol.*, vol. 69, no. 5, pp. 4763–4772, May 2020.
[44] S. Kirkpatrick, C. D. Gelatt, and M. P. Vecchi, "Optimization by simulated annealing," *Science*, vol. 220, no. 4598, pp. 671–680, 1983.
[45] W. Zhao, Z. Zhang, and L. Wang, "Manta ray foraging optimization: An effective bio-inspired optimizer for engineering applications," *Eng. Appl. Artif. Intell.*, vol. 87, Jan. 2020, Art. no. 103300.
[46] U. Eminoglu and M. H. Hocaoglu, "Distribution systems forward/backward sweep-based power flow algorithms: A review and comparison study," *Electr. Power Compon. Syst.*, vol. 37, no. 1, pp. 91–110, Dec. 2008.
[47] A. El-Fergany, "Optimal allocation of multi-type distributed generators using backtracking search optimization algorithm," *Int. J. Electr. Power Energy Syst.*, vol. 64, pp. 1197–1205, Jan. 2015.

[48] H. Abdel-mawgoud, S. Kamel, M. Ebeed, and A.-R. Youssef, "Optimal allocation of renewable DG sources in distribution networks considering load growth," in *Proc. 19th Int. Middle East Power Syst. Conf. (MEPCON)*, Dec. 2017, pp. 1236–1241.

[49] E. S. Ali, S. M. A. Elazim, and A. Y. Abdelaziz, "Ant lion optimization algorithm for renewable distributed generations," *Energy*, vol. 116, pp. 445–458, Dec. 2016.

[50] M. M. Aman, G. B. Jasmon, A. H. A. Bakar, and H. Mokhlis, "A new approach for optimum simultaneous multi-DG distributed generation units placement and sizing based on maximization of system loadability using HPSO (hybrid particle swarm optimization) algorithm," *Energy*, vol. 66, pp. 202–215, Mar. 2014.

[51] E. Lopez, H. Opazo, L. Garcia, and P. Bastard, "Online reconfiguration considering variability demand: Applications to real networks," *IEEE Trans. Power Syst.*, vol. 19, no. 1, pp. 549–553, Feb. 2004.

[52] W. Price, S. G. Casper, C. O. Nwankpa, R. W. Bradish, H. D. Chiang, C. Concordia, J. V. Staron, C. W. Taylor, E. Vaahedi, and G. Wu, "Bibliography on load models for power flow and dynamic performance simulation," *IEEE Power Eng. Rev.*, vol. 15, no. 2, p. 70, Feb. 1995.

[53] S. H. Jangamshetti and V. G. Rau, "Site matching of wind turbine generators: A case study," *IEEE Trans. Energy Convers.*, vol. 14, no. 4, pp. 1537–1543, Dec. 1999.

[54] A. Ali, K. Mahmoud, D. Raisz, and M. Lehtonen, "Probabilistic approach for hosting high PV penetration in distribution systems via optimal oversized inverter with watt-var functions," *IEEE Syst. J.*, vol. 15, no. 1, pp. 684–693, Mar. 2021.

[55] S. X. Chen, H. B. Gooi, and M. Q. Wang, "Sizing of energy storage for microgrids," *IEEE Trans. Smart Grid*, vol. 3, no. 1, pp. 142–151, Mar. 2012.

[56] H. Abdel-Mawgoud, S. Kamel, M. Ebeed, and M. M. Aly, "An efficient hybrid approach for optimal allocation of DG in radial distribution networks," in *Proc. Int. Conf. Innov. Trends Comput. Eng. (ITCE)*, Feb. 2018, pp. 311–316.

[57] N. C. Sahoo and K. Prasad, "A fuzzy genetic approach for network reconfiguration to enhance voltage stability in radial distribution systems," *Energy Convers. Manage.*, vol. 47, nos. 18–19, pp. 3288–3306, Nov. 2006.